FORM TI-12
8/94

WAPD-T-3135

CONF-970691--1

# ANALYTICAL PREDICTION OF THE LOCATION OF DUCTILITY DIP CRACKING IN THE TRANS-VARESTRAINT TEST

Ishar Singh, Wayne Kroenke, Mark Cola



U. S. Department of Energy
Contract DE-AC11-93PN38195





BETTIS ATOMIC POWER LABORATORY WEST MIFFLIN, PENNSYLVANIA 15122-0079

Operated for the U.S. Department of Energy
by WESTINGHOUSE ELECTRIC CORPORATION

# DISCLAIMER

# ANALYTICAL PREDICTION OF THE LOCATION OF DUCTILITY DIP CRACKING IN THE TRANS-VARESTRAINT TEST

ISHAR SINGH AND WAYNE KROENKE - WESTINGHOUSE BETTIS
MARK COLA - WESTINGHOUSE MAO

## INTRODUCTION

Some NiCrFe weld metals exhibit decreased ductility over a temperature range known as the "ductility dip" temperature (DDT) range. Ductility dip cracking (DDC) is a phenomenon which occurs in a zone bounded by the DDT range on its sides and a threshold plastic strain on its bottom as shown in figure 1. Figure 1 illustrates how ductility varies as weld metal cools from the solidus temperature for materials with and without a ductility dip.

The purpose of this work is to demonstrate the ability to predict the location of the DDC in a Trans-Varestraint Test (TVT) for a specimen machined from a weld deposited EN52 plate. The DDC predictions require a combination of Trans-Varestraint testing and finite element analysis. The test provides the threshold value of externally applied nominal strain below which DDC does not occur. The analysis provides the corresponding threshold local or peak strain. The threshold local plastic strain level and the DDT range are used to predict the location of the DDC. The ultimate purpose of this work is to evaluate susceptibility of highly constrained, component welds to DDC.

Test results for Trans-Varestraint Testing for a weld deposited EN52 plate are reported in reference [1]. The ability to predict the location of the DDC in the Trans-Varestraint Test using the techniques reported herein is demonstrated by showing good comparison between the analytical results and the test data.

## DESCRIPTION OF TVT

The TVT simulates the large shrinkage strains characteristic of a highly constrained component weld. As described in reference [2], the test employs a weld bead to produce thermal strains characteristic of the welding process and weld heat input to produce microstructures virtually identical to actual production welds. Mechanical strains simulating restraint are provided by an externally applied augmented strain. The test allows considerable flexibility, since the microstructure and mechanical factors can be varied independently.

For the work reported herein, the TVT test specimen and set up are shown schematically in figure 2. The thermal strains and heat input are provided by an autogenous gas tungsten arc weld bead. The mechanical or augmented strain is provided by bending the specimen over a die block whose radius is fixed by the desired magnitude of augmented strain. The test is executed by starting the weld torch travel and then applying the augmented strain by bending the specimen over the die block using the deflection controlled stroke of a loading frame. Figure 3 show the TVT thermal and mechanical loading. Figure 3a shows the travel of the weld torch which comes on at zero seconds, travels at a constant rate of 152.4 mm/minute, and shuts off at

11.8 seconds. Figure 3b shows the applied deflection which starts at 7.1 seconds, increases linearly to its maximum value (referred to as the augmented strain ramp), and then remains constant for the remainder of the test. The time required to reach the desired magnitude of augmented strain is controlled by the stroke rate (i.e. rate at which plate is deflected). For the TVT investigated herein, the specimen material and thermal parameters (heat input and torch travel speed and travel distance) remained constant while the mechanical parameters (augmented strain magnitude and stroke rate) were varied as listed in table 1.

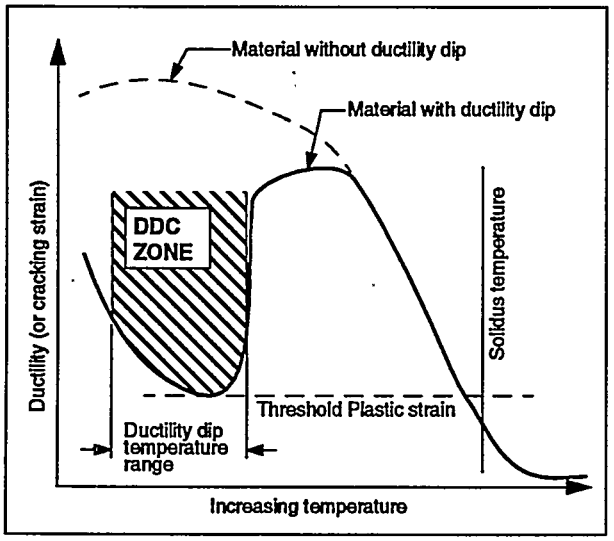


Figure 1. Material exhibiting a ductility dip

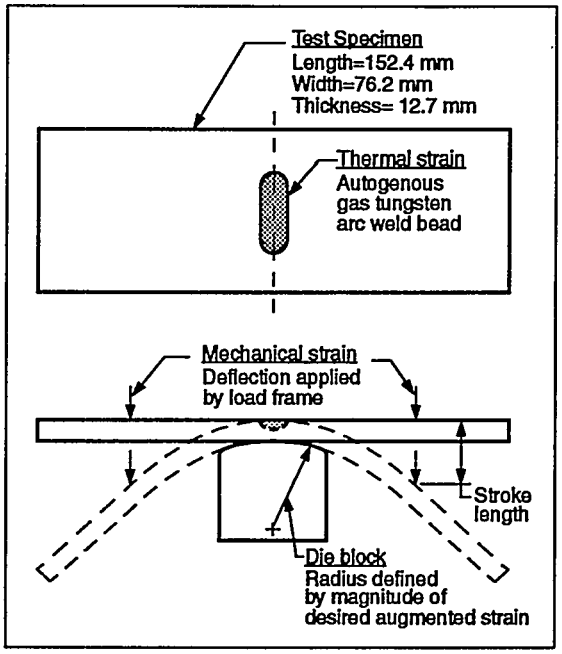


Figure 2. Test set up

## ANALYSIS OF EN52 TVT

A three dimensional finite element residual stress analysis was used to determine the local plastic strain as a function of the augmented strain magnitude and the stroke rate. The finite element model in the vicinity of the weld pool is shown in figure 4. The material properties used for the entire model are for NiCrFe EN52 weld deposited metal as listed in table 2. The properties at high temperatures are a good representation of the material behavior but are based on limited data. One heat transfer analysis of the weld thermal transient provided the temperature history at each node for all the subsequent strain solutions. Multiple strain solutions were used to determine local plastic strains as functions of the augmented strain magnitudes and the TVT stroke rates of table 1.

Since no filler metal is deposited during the autogenous weld, the thermal and strain solutions modeled reheating of existing material without the addition (birthing) of finite elements. Also, it was not necessary to model volumetric changes due to phase changes, since EN52 does not experience a solid state phase change during solidification. Two phenomena included were latent heat in the thermal solution and annealing of plastic strains in the strain solutions. Annealing occurs when solid material with plastic strains is remelted and restored to its virgin state. In the computer simulation, any time the temperature at a finite element integration point reached or exceeded the liquidus temperature, the plastic strains and strain hardening effects were zeroed out and stayed zeroed out until the temperature of the integration point dropped below the liquidus temperature. A potential alternative procedure of zeroing out the plastic properties at the solidus rather than the liquidus temperature would have provided similar results, since the difference between the

solidus and liquidus temperatures is only 34°C. The procedure of zeroing out plastic quantities when the temperature exceeds the liquidus temperature does not include the annealing which occurs below the

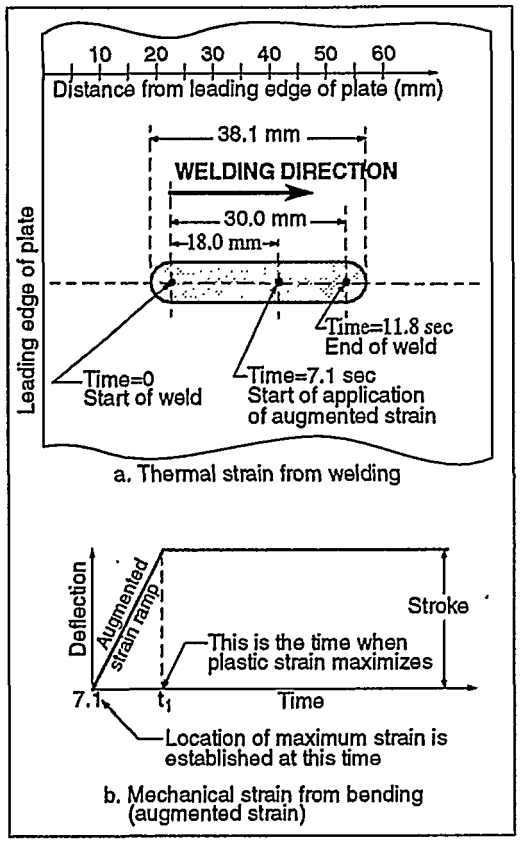


Figure 3. Applied strain

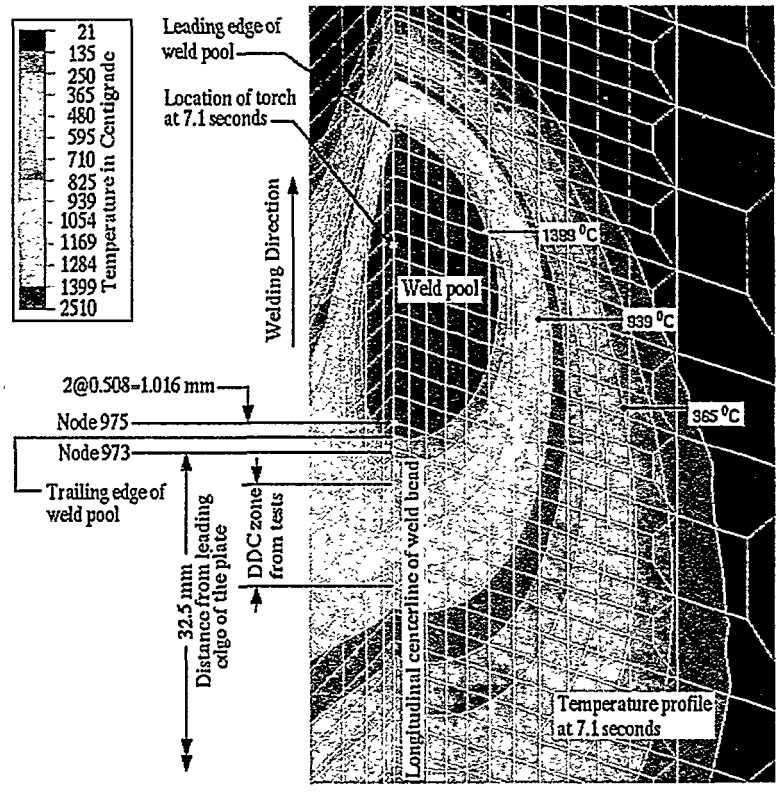


Figure 4. Typical temperature distribution

liquidus temperature. This latter annealing has a much smaller effect than the above-liquidus-temperature annealing especially at the trailing edge of the molten pool which is the focus of this study.

## THERMAL SOLUTION

The thermal analysis was performed using ABAQUS [3]. Symmetry boundary conditions were assumed on the plane normal to the plate and containing the weld centerline. All other surfaces had natural convection in addition to radiation effects. The heat input from the welding torch was modeled by a moving heat flux boundary condition. The magnitude and distribution of heat flux on the top surface of the plate were based on the analytical and experimental studies reported in reference [4]. The magnitude of the total heat input rate Q, on the plate surface is given by $Q = \eta EI$ where $\eta$ is the arc efficiency (70 percent assumed), E is the arc voltage (13.5 volts), and I is the arc current (180 amperes). At all times, the surface heat flux distribution modeling the arc heat distribution was assumed to be a radially symmetric normal distribution as defined below:

$$q(r) = \frac{3Q}{\pi R^2}\exp\left\{-3\left(\frac{r}{R}\right)^2\right\}$$

where r is the radial distance from the instantaneous center of the heat source and R is the characteristic radial dimension distribution parameter with a value of 6.91mm per reference [4]. Other parameters that entered

into the evaluation were a latent heat of 67.87 cal/gm, solidus temperature of 1365°C, and liquidus temperature of 1399 °C.

Typical temperature distribution profiles on the top surface and symmetry plane are shown in figures 4 and 5. Figure 4 shows the tear shaped molten weld pool and isotherms at 7.1 seconds which is the time of the start of the augmented strain ramp. The shape of the molten pool changes with torch travel. Figure 5 shows the temperature distribution on the top surface along the weld center line at the start (7.1 seconds) of the augmented strain ramp, at two intermediate times, at the time the torch is turned off (11.8 seconds), and for three times after the torch is turned off. For the work reported herein there were no measured temperatures to directly confirm the calculated results. On the other hand, the temperature distribution obtained is partially qualified by the fact that the calculated temperatures and observed cracks correlated and that the calculated size of the molten pool on the top surface was similar to the measured size of the molten pool in the TVT specimens. As discussed later and shown in figure 4, the predicted DDT range locations agree with the observed DDC locations. The small bump in the on-cooling side of the temperature distribution of the figure 5 curves between the solidus (1365°C) and liquidus (1399 °C) temperatures results from the latent heat.

Conclusions concerning the thermal analysis are the following:

1. The calculated temperature distributions are indirectly confirmed by the fact that the location of the calculated DDT range corresponds to observed cracking locations.
2. The temperature profile on the top surface along the weld center line is almost constant and moves at the speed of the heat source. The shape of the on-heating half of the profile stays constant during the torch travel; whereas, the shape of the on-cooling half changes somewhat. The shape of the on-cooling curve changes, because the heat transfer is due to conduction only without the effect of the torch heat flux which is driving the on-heating portion of the distribution.
3. Latent heat effects are small as seen by the local deviation in the slope of the temperature profile between the solidus and liquidus temperatures.

## STRAIN SOLUTION

The residual strain analysis was performed using a Bettis structural analysis program. Small deflection analysis was used, since preliminary analyses indicated that large deflection solutions are not required and since significant computer time could be saved by using the small deflection formulation. Symmetry boundary conditions were used on the plane normal to the plate and containing the weld centerline. The plastic strain reported herein is the generalized local plastic strain defined as $\epsilon_g = \sqrt{2/3\ \epsilon_{ij}\ \epsilon_{ij}}$ where $\epsilon_{ij}$ is the plastic strain tensor.

Due to the high temperatures along the weld bead, the TVT specimen of this study did not bend uniformly around the die block but developed a kink at the weld centerline which has strains 2 to 3 percent larger than the augmented strain. This deflected shape causes the specimen to lift off the die block at the center. For the analysis, the augmented strain was introduced by applying displacements to the nodes that are common to the specimen and the die block. A manual iteration procedure was used to determine which nodes were in contact with the die block and which nodes near the weld centerline had lifted off. Comparison between

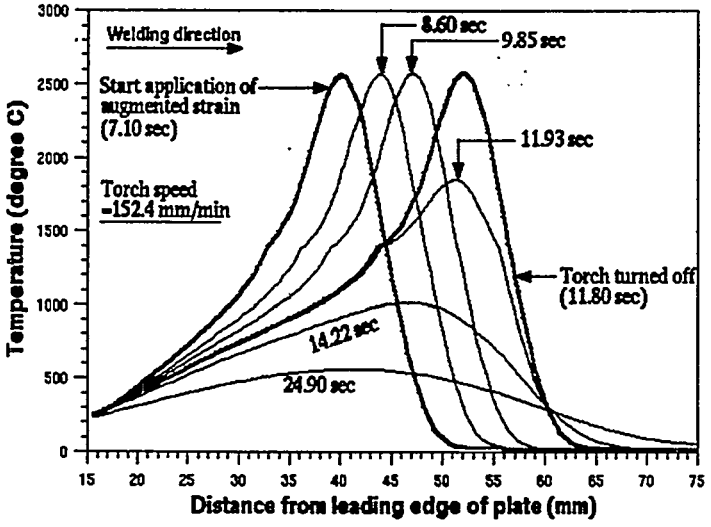


Figure 5. Temperature distribution along center line of weld

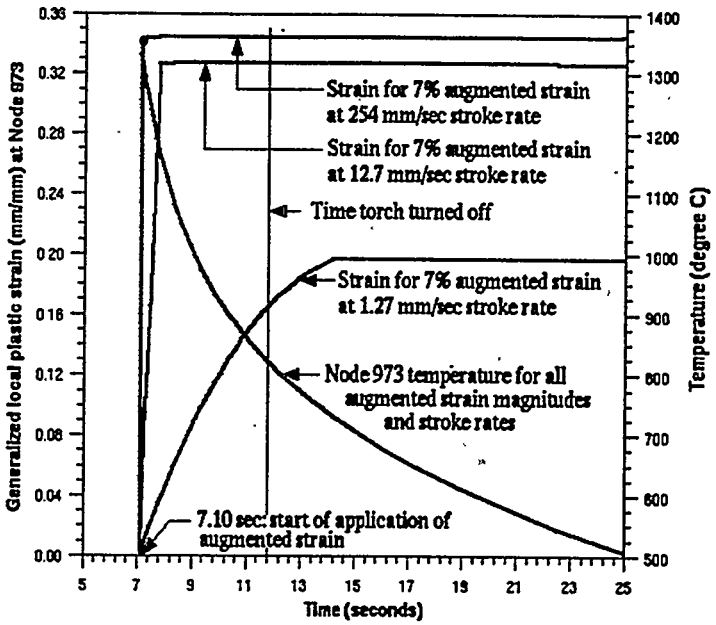


Figure 6. Variation of temperature and strain with time

analysis and testing results for the nominal deflected shape in the region of the die block confirmed the acceptability of this manual procedure. A more accurate technique that will be used in the future is to use contact-type elements at the plate-to-die block interface.

Representative variations of local plastic strain are shown in figures 6 and 7. Figure 6 provides the behavior of node 973 of the analyses reported herein. As will be discussed below, this location is significant, since the maximum local strain is always located at node 973 regardless of the augmented strain magnitude or the stroke rate. Node 973 is 0.508 mm behind the trailing edge of the molten pool at the start of the augmented strain ramp as shown in figure 4. Figure 6 shows the node 973 variation of local plastic strain with time as a function of stroke rate for an augmented strain of 7 percent. For each strain curve the maximum local plastic strain is reached at the end of the augmented strain ramp which is the start of the horizontal line shown in figure 6 for each stroke rate. Node 973 temperature variation with time is also shown. Figure 6 shows that the maximum local plastic strain increases from 20 to 34 percent as the stoke rate increases from 1.27 to 254 mm/second. For the faster two stroke rates, the maximum local plastic strain is reached in less than a second while the torch is still on. For the slower stroke rate, it takes longer to reach the maximum local strain which occurs after the torch has been turned off and the material is cooling. The lower temperature and corresponding stronger material along the weld center line causes the maximum local plastic strain to be smaller than for the faster two stroke rates. The node 973 temperature is the same for all three stroke rates. This emphasizes the TVT characteristic that the thermal strains are independent of the mechanical strains and have negligible magnitudes compared to the mechanical strains.

Figure 7 shows the variation of the local plastic strain with distance from the leading edge of the plate as a function of augmented strain magnitude and stroke rate. The magnitude and time for the maximum local plastic strain as a function of augmented strain magnitude and stroke rate are given in table 1. Only the

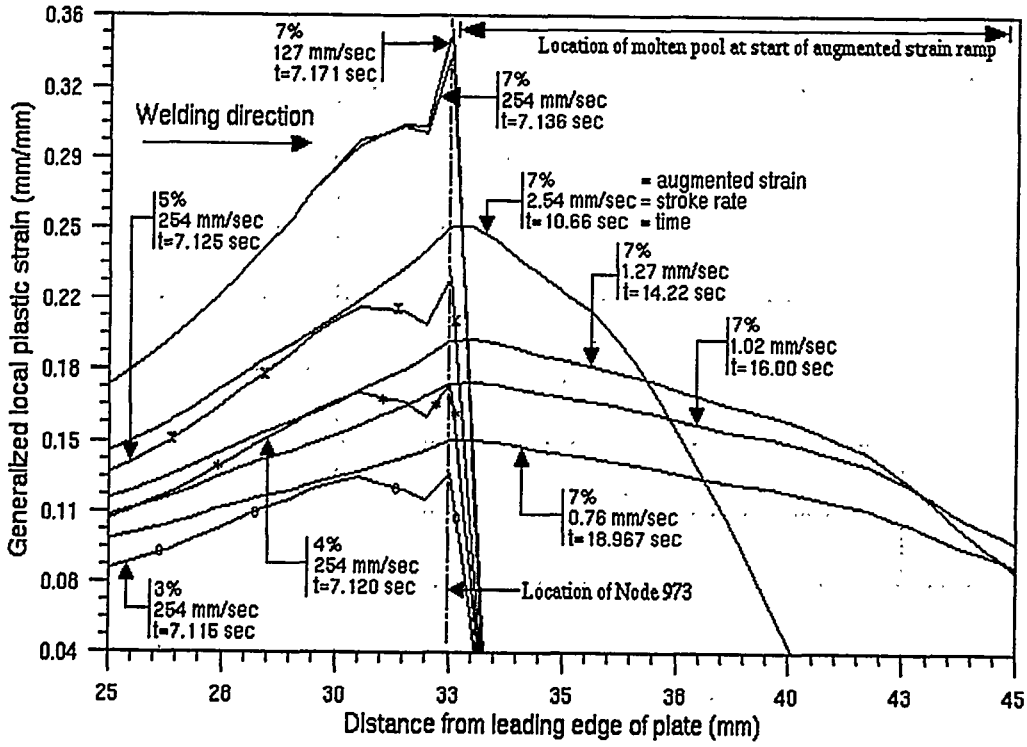


Figure 7. Variation of strain distribution with augmented strain and bend rate

on-cooling portion of the curve (follows trailing edge of the molten pool) is shown, since this is where the DDC occurs. As stated in the previous paragraph, it can be seen that the maximum local plastic strain always occurs just behind the trailing edge of the molten pool location that exists at the start (7.1 seconds) of the application of the augmented strain ramp. (The edge of the molten pool is defined as the liquidus temperature isotherm bounding the molten pool.) For the finite element grid used for the analyses reported herein, this point of maximum local plastic strain was 0.508 mm behind the trailing edge at node 973. In addition to showing the location of the maximum local plastic strain, figure 7 also shows that the maximum local plastic strain increases from 12 to 34 percent as the stoke rate increases from 0.51 to 254 mm/second and from 13 to 34 percent as the augmented strain magnitude increases from 3 to 7 percent. For the faster stroke rates (rates greater than 1.27 mm/second), the strain is zero for distances within the molten pool, because temperatures are greater than the liquidus temperature. For the slower stroke rates the strains are nonzero, because the temperatures over the distances shown are less than the liquidus temperature. The temperatures are less than the liquidus temperature, because the torch is turned off before the end of the augmented strain ramp which corresponds to the local plastic strain curves of figure 7.

Conclusions concerning the strain analysis are the following:

1. The location of maximum local plastic strain along the center line of the weld is always located at the trailing edge of the molten pool location that exists at the start of the application of the augmented strain.
2. The magnitude of the maximum local plastic strain increases with an increase in the magnitude of the augmented strain and with an increase in the stroke rate. This latter trend occurs, because the slower stroke rate results in a majority of the augmented strain being applied to a lower temperature, stronger material. As shown in table 1, this latter trend also has an upper limit of approximately 25.4 mm/second

above which increasing the stroke rate does not cause any further increases in maximum local plastic strains.

3. Once the maximum local plastic strain is reached at a location at the end of the augmented strain ramp, its magnitude is almost constant over the TVT period.

## THRESHOLD LOCAL PLASTIC STRAIN

The threshold local plastic strain and DDT range are used to predict the location of DDC. The threshold local plastic strain is determined from an analysis of the TVT specimen subjected to the threshold augmented strain. For the NiCrFe EN52 material being evaluated herein, the augmented strain magnitude at which DDC appeared was 4 percent with a stroke rate of 254 mm/second as reported in reference [1]. TVT specimens with less than 4 percent augmented strain at a stroke rate of 254 mm/second did not experience any DDC.

The threshold local plastic strain is the maximum local plastic strain determined by analysis to exist in the region susceptible to DDC (i.e. the region just behind the trailing edge of the molten pool). For the testing reported herein, the length of the ductility dip cracks in the specimen with threshold augmented strains is a fraction of a millimeter. The assumption is made that this short crack will occur at the location of maximum local plastic strain. This maximum local plastic strain value is used as the threshold local plastic strain. Remembering that the strain magnitudes at a given location do not change after the end of the application of the augmented strain and that the location of the maximum local plastic strain will cool through the DDT

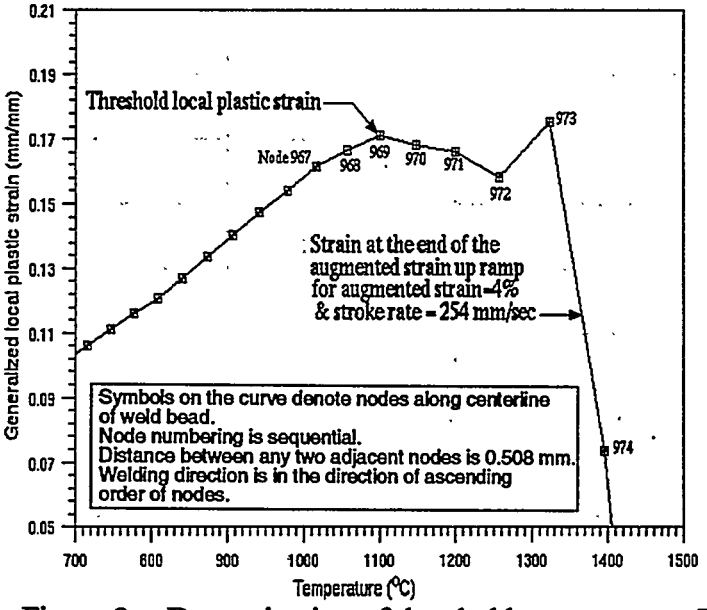


Figure 8. Determination of threshold local plastic strain

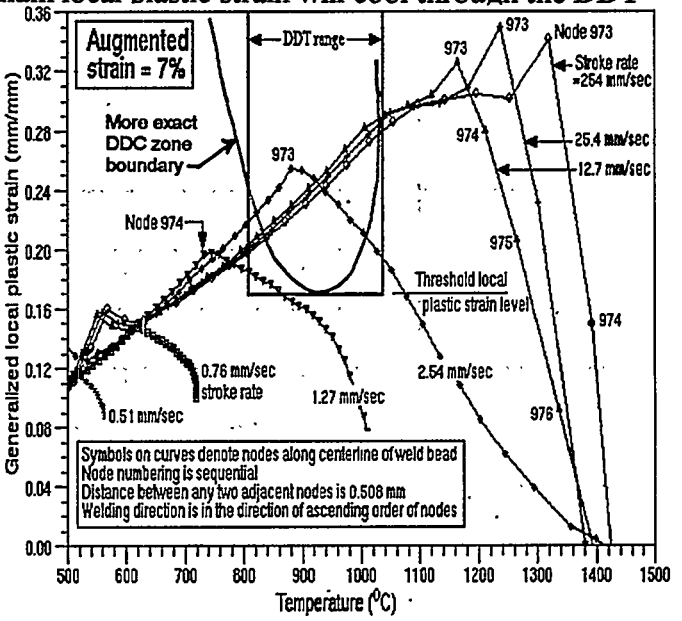


Figure 9. Determination of cracking location and distance

range as the weld solidifies, leads to the conclusion that the material at the location of the maximum local plastic strain will be subjected to the largest strain during the cooling through the DDT range such that it would be the most likely place for the first short crack to form. For the strain curve of figure 8, the maximum local plastic strain in the region susceptible to DDC is at node 969. A known characteristic of DDC is that it occurs away from the weld fusion zone. In this case, node 969 is about 2.5 mm from the weld fusion zone

which is at node 974 (see figure 4). Based on these considerations, the threshold local plastic strain required to cause DDC in the EN52 TVT specimen is 17 percent.

## DUCTILITY DIP CRACKING EVALUATION

Based on the 4 percent threshold augmented strain defined by reference [1], the 17 percent threshold local plastic strain determined above, and the DDT range, the location of DDC was predicted for TVT specimens with augmented strains of 7 percent and a range of stroke rates. Figure 9 shows the local plastic strain analysis results. The DDC zone is shown between the DDT range of 815 and 1040 °C and above the threshold local plastic strain of 17 percent. The DDT range between 815 and 1040 °C was proposed by reference [1]. The portion of the strain curve within the DDC zone represents material susceptible to DDC. Since each point used to plot these strain curves represents a node on the top surface at the weld centerline, the node numbers within the DDC zone can be correlated with lengths on the TVT specimen.

Solutions for stroke rates of 25.4 mm/second and higher have very similar strain curves within the DDC zone and, therefore, predict cracking over similar distances. Solutions for stroke rates between 1.27 and 12.7 mm/second have a variable number of nodes and consequently variable distances susceptible to DDC. Since

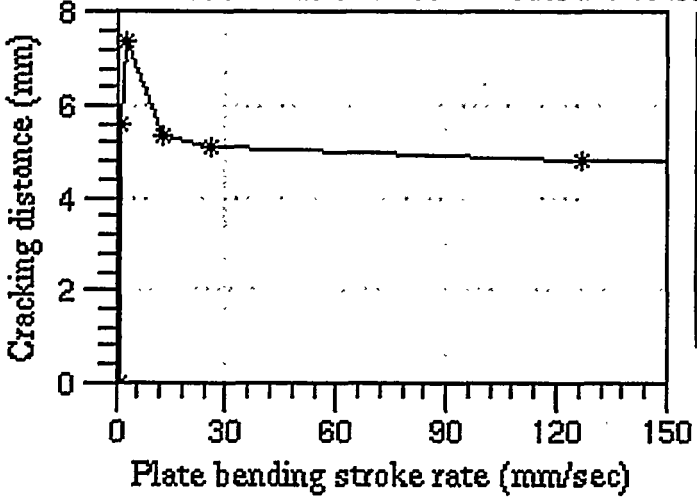


Figure 10. Variation of cracking distance with stroke rate

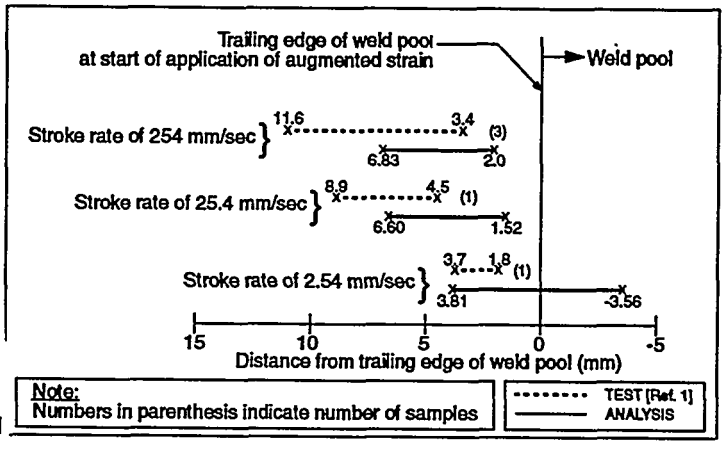


Figure 11. Crack distance comparison

solutions with stroke rates between 0.51 and 1.02 mm/second have no nodes within the DDC zone, DDC is not predicted for these stroke rates. The variation of the distance over which DDC is predicted is shown in figure 10 where it is seen that the distance over which cracking is predicted starts at zero with slow stroke rates, peaks at a stroke rate of approximately 2.54 mm/sec., and takes on a constant distance for stroke rates greater than 25.4 mm/sec.

DDC locations predicted by analysis and observed in the testing of reference [1] are compared in figure 11 for stroke rates of 2.54, 25.4, and 254 mm/second. It can be seen that the predicted and observed DDC locations are similar and that the DDC locations are a function of the stroke rate. Reference [5] indicates that the DDT range is a function of the plastic strain magnitude as shown by the parabolic DDC zone of figure 9. Data of this type is not available for EN52 weld metal. If the DDC zone has a shape more like the parabola, the figure

11 comparison would be improved, since the analytical distance of crack locations would be reduced for the slower stroke rates and increased for the faster stroke rates.

Another good correlation between analytical and observed cracking results occurred for 7 percent augmented strain and the slow stroke rates. Analysis predicted that there would be no DDC when the stroke rate was at or below 1.02 mm/second. From TVT there was no DDC for stroke rates at or below 1.14 mm/second.

## SUMMARY AND CONCLUSIONS

Analysis techniques can predict local plastic strains adjacent to the molten pool. These techniques provide the basis for the evaluation of the Trans-Varestraint Test, reported herein, and for component weld evaluations.

Analysis, in combination with Trans-Varestraint Test data, can be used to predict the location of the ductility dip cracking in a Trans-Varestraint Test specimen. The cracking locations in the Trans-Varestraint Test can be determined by locating regions that satisfy two criteria: (1) the calculated local plastic strain is greater than the threshold local plastic strain and (2) the temperatures are within the ductility dip temperature range.

Analysis, in combination with Trans-Varestraint Test data, can be used to determine the threshold local plastic strain for ductility dip cracking. The threshold local plastic strain for ductility dip cracking is the local plastic strain that occurs at the location of the ductility dip cracking in the threshold augmented strain specimen. For the weld deposited EN52 specimens analyzed herein, the threshold local plastic strain is 17 percent.

The magnitude of the maximum local plastic strain increases with an increase in the magnitude of the augmented strain and with an increase in the stroke rate.

Analysis shows that the location of the maximum local plastic strain along the center line of the weld for the TVT is always at the trailing edge of the molten pool that exists at the start of the augmented strain ramp. This finding is similar to the Longitudinal Varestraint Test result reported in 1982 in reference [6]: "Varestraint Tests normally reveal that the hot-cracking produced is invariable adjacent to, and usually contiguous with, the location of the weld puddle at the instant of application of the augmented strain."

Techniques used herein to predict the ductility dip cracking locations for the Trans-Varestraint Test specimen are proposed for application to highly constrained, component welds.

## REFERENCES


1. Mark Cola and W. Lin, "Weldability of Inconel Filler Metal 52," to be presented at the Seventy-Eighth Annual AWS Convention, April, 1997 with subsequent publication in the AWS Journal.
2. Carl D. Lundin, R. Menon, C. H. Lee, and V. Osorio, "New Concepts in Varestraint Testing for Hot Cracking," ASM, Welding Research: The State of the Art, Proceedings of the JDC University Research Symposium, 1985, Ontario, Canada, pp 33-42.
3. ABAQUS User's Manual, version 5.4, Hibbit, Karlsson & Sorensen Inc., 1800 Main Street, Pawtucket, Rhode Island, 1994.
4. S. S. Glickstein and E. Friedman, "Temperature Transients in Gas Tungsten - arc Weldments," Welding Review, 72, May 1983.

5. D. McKeown, Quantifying Weldability - Hot Cracking, Proceedings of Seminar on Quantifying Cracking, Coventry, UK, October 10, 1985. Editor R. J. Pargeter, Published by Abington, Cambridge, CB1 6AL, UK; The Welding Institute, 1988, Paper 3, pp. 45-58.
6. C. D. Lundin, A. C. Lingenfeller, G. E. Grotke, G. G. Lessmann, S. J. Matthews, "The Varestraint Test," Welding Research Council Bulletin 280, August, 1982.

**TABLE 1. VARIATION OF MAXIMUM PLASTIC STRAIN WITH AUGMENTED STRAIN AND STROKE RATE**

| AUGMENTED STRAIN (PERCENT) | STROKE RATE (MM/SECOND) | MAXIMUM LOCAL PLASTIC STRAIN (PERCENT) | TIME FOR MAXIMUM LOCAL PLASTIC STRAIN (SECONDS) |
|---|---|---|---|
| 3 | 254 | 13 | 7.12 |
| 4 | 254 | 18 | 7.12 |
| 5 | 254 | 23 | 7.13 |
| 7 | 0.508 | 12 | 24.90 |
| | 0.762 | 15 | 18.97 |
| | 1.016 | 18 | 16.00 |
| | 1.27 | 20 | 14.22 |
| | 2.54 | 25 | 10.66 |
| | 12.7 | 33 | 7.81 |
| | 25.4 | 35 | 7.46 |
| | 127 | 35 | 7.17 |
| | 254 | 34 | 7.14 |

**TABLE 2. PARTIAL EN52 WELD METAL MATERIAL PROPERTIES**

| PROPERTY | TEMPER-ATURE (°C) | VALUE | |
|---|---|---|---|
| Thermal conductivity [cal/sec-cm-°C] | 21 | 2.448 E-02 | |
| | 816 | 6.404 E-02 | |
| | 1649 | 9.902 E-02 | |
| Specific heat [cal/g-°C] | 21 | 0.1042 | |
| | 816 | 0.1573 | |
| | 1649 | 0.1923 | |
| Density [g/cm$^3$] | 21 | 8.207 | |
| | 816 | 7.947 | |
| | 1649 | 7.742 | |
| Thermal expansion [mm/mm-°C] | 21 | 13.763 E-06 | |
| | 816 | 14.927 E-06 | |
| | 1649 | 15.665 E-06 | |
| Elastic modulus [MPa] | 21 | 175 E+03 | |
| | 816 | 125 E+03 | |
| | 1649 | 55.2 E+03 | |
| | | true strain [mm/mm] | true stress [MPa] |
| Plastic stress-strain relations | 21°C | 0.000 | 454 |
| | | 0.497 | 1,047 |
| | 816 | 0.000 | 218 |
| | | 0.497 | 454 |
| | 1649 | 0.000 | 4.14 |
| | | 0.497 | 4.14 |